SEMARAK ILMU PUBLISHING

Semarak Engineering Journal

Journal homepage:
https://semarakilmu.com/
ISSN: 3036-0145



Comparison of the Fluid Velocity of Water (H_2O), Ammonia (NH_3), and Mercury (Hg) in Pipes using ANSYS Simulation

Aulia Ayu Safira[1], Cut Widia Catur Rose[1], Dila Larasati[1], Hana Hanifah Raharjo[1], Satria Bagas Nur Setyo[1], Singgih Dwi Prasetyo[1,*]

[1] Power Plant Engineering Tchnology, Faculty of Vocational Studies, State University of Malang, 65145 Malang, Indonesia

ARTICLE INFO

Article history:
Received 8 October 2024
Received in revised form 30 October 2024
Accepted 2 November 2025
Available online 5 November 2025

Keywords:
Pipe; fluid velocity; mercury; water; ammonia

ABSTRACT

The flow behavior of fluids in piping systems is a fundamental aspect of thermal and hydraulic engineering, influencing numerous industrial processes such as cooling, heat transfer, and fluid transport. This study presents a comparative analysis of the flow velocity of three fluids—water, ammonia, and mercury —within a pipe using Computational Fluid Dynamics (CFD) simulations conducted in ANSYS Fluent. Each fluid was tested under identical geometric and boundary conditions to isolate the effects of density and viscosity on flow characteristics. The pipe model consisted of a straight section with an elbow, designed to observe changes in velocity distribution as the fluid changed direction. Simulation results revealed that all three fluids exhibited nearly identical average outlet velocities, with values of 0.520096 m/s for water, 0.520217 m/s for ammonia, and 0.520088 m/s for mercury. Despite slight variations in viscosity and density, the maximum difference between these values was only 0.0248%, indicating a negligible influence of fluid type on average flow velocity when inlet conditions are constant. Ammonia displayed the highest peak velocity due to its lower viscosity, while mercury showed the lowest as a result of its higher density. Overall, the study concludes that variations in fluid properties have minimal impact on velocity distribution under steady inlet velocity. Future research is recommended to explore the effects of temperature, pipe roughness, and turbulence to better understand fluid flow behavior in more complex industrial systems.

1. Introduction

Fluid flow piping system is a key topic in thermal and hydraulic engineering, significantly influencing many essential industrial processes. These processes include the distribution of water and the management of refrigerants like ammonia in cooling systems [1], as well as the operation of state-of-the-art nuclear reactor cooling systems that utilize liquid metals such as mercury or various alloys [2]. To comprehend and forecast this flow behavior, precise solutions are required; however, the intricate nature of the Navier-Stokes equations under turbulent conditions or within complex shapes often prevents straightforward analytical solutions [3]. Consequently, Computational Fluid Dynamics,

* *Corresponding author.*
E-mail address: singgih.prasetyo.fv@um.ac.id

or CFD, has become an effective numerical method for simulating fluid behavior, allowing for the visualization and thorough examination of essential parameters like flow velocity distributions [4]. The use of CFD has demonstrated its effectiveness in forecasting flow properties and heat transfer, establishing it as a common approach in contemporary engineering design [5,6].

Research into pipe flow has been thoroughly explored, but the majority of investigations concentrate on water or standard fluids [7,8]. Refrigerants like ammonia are frequently examined in relation to heat transfer and phase change [9], while liquid metals such as mercury, known for their excellent electrical and thermal conductivity, are usually studied independently, often highlighting Magneto hydrodynamic (MHD) influences or issues related to turbulent heat transfer [10]. Crucially, when the inlet velocity (V_{inlet}) is fixed as a boundary condition, the average flow velocity (V_{avg}) at the outlet is mathematically constrained by the principle of mass conservation (Continuity Equation), dictating that the results should be nearly identical regardless of the fluid type. Therefore, the primary scientific contribution of this study is not to compare the V_{avg} values, which are predictable. Instead, a critical scarcity exists in integrated studies that evaluate how the significantly contrasting physical properties (low viscosity of ammonia vs. high density of mercury) manifest within the internal hydrodynamic structure under identical flow conditions [11,12]. This gap necessitates systematic comparative evaluations focusing on the axial velocity profiles, the local velocity gradient, and the determination of the flow regime (Reynolds Number, Re) as key differentiating factors [13,14].

The originality of this study, therefore, lies in its rigorous comparison between Water (standard reference), Ammonia (low-viscosity refrigerant), and Mercury (high-density liquid metal) within a circular pipe. The vast disparities in density and viscosity among these three fluids are not expected to significantly alter the average velocity, but rather the internal flow structure. These differences are anticipated to lead to distinct variations in the Reynolds Number (Re), the shape of the velocity profile (e.g., parabolic vs. flatter flow), the magnitude of wall shear stress, and the proximity to the transitional flow regime [15]. The core objective of this research is thus to quantitatively characterize the unique hydrodynamic signatures of these three fluids under identical conditions. This is achieved by performing a comparative evaluation of the flow velocity profiles and Re values through CFD simulations, providing insights beyond a simple report of average flow rates.

Building upon this objective, the present study employs ANSYS Fluent to model and analyze the flow behavior of water, ammonia, and mercury within a circular pipe under identical boundary and geometric conditions. A systematic methodology is adopted, where each fluid is simulated using consistent inlet velocity and pressure parameters to isolate the critical effects of density and viscosity on the internal velocity gradient and flow regime [16]. Through numerical analysis, the study aims to visualize velocity contours, quantify the difference in Reynolds Number Re, and assess the variations in flow development along the pipe. Ultimately, the results are expected to provide engineers with critical insight into when a fluid's inherent physical properties begin to dominate the flow dynamics over imposed boundary conditions, thereby supporting the design and optimization of more accurate and efficient industrial piping systems [17].

2. Methodology

2.1 Research Approach

This research was conducted through a series of structured steps as illustrated in Figure 1. The initial stage was problem identification, which aimed to determine the main focus of the research on comparative analysis of the flow velocity of three types of fluids, namely water (H_2O), ammonia (NH_3), and mercury (Hg), in pipes [18]. After that, a literature review was conducted to gather theoretical

foundations related to fluid dynamics, laminar and turbulent flow characteristics, and the basic principles of Computational Fluid Dynamics (CFD) [19]. The next step involved modeling and simulation using ANSYS Fluent software, where a cylindrical pipe geometry was created and meshed to obtain precise numerical results. The three types of fluids were then simulated in the same pipe model to ensure that the comparison conditions remained uniform and valid. Next, simulations were run for each fluid using identical boundary conditions, such as inlet velocity and pressure. The simulation results were then analyzed to observe the flow velocity distribution pattern and fluid characteristics affected by differences in physical properties, including density and viscosity. Calculations were performed to determine the average flow velocity and display the visualization pattern using contour plots and velocity vectors [20]. In the final stage, all results were analyzed thoroughly to draw conclusions about the effect of fluid type on flow velocity in pipes.

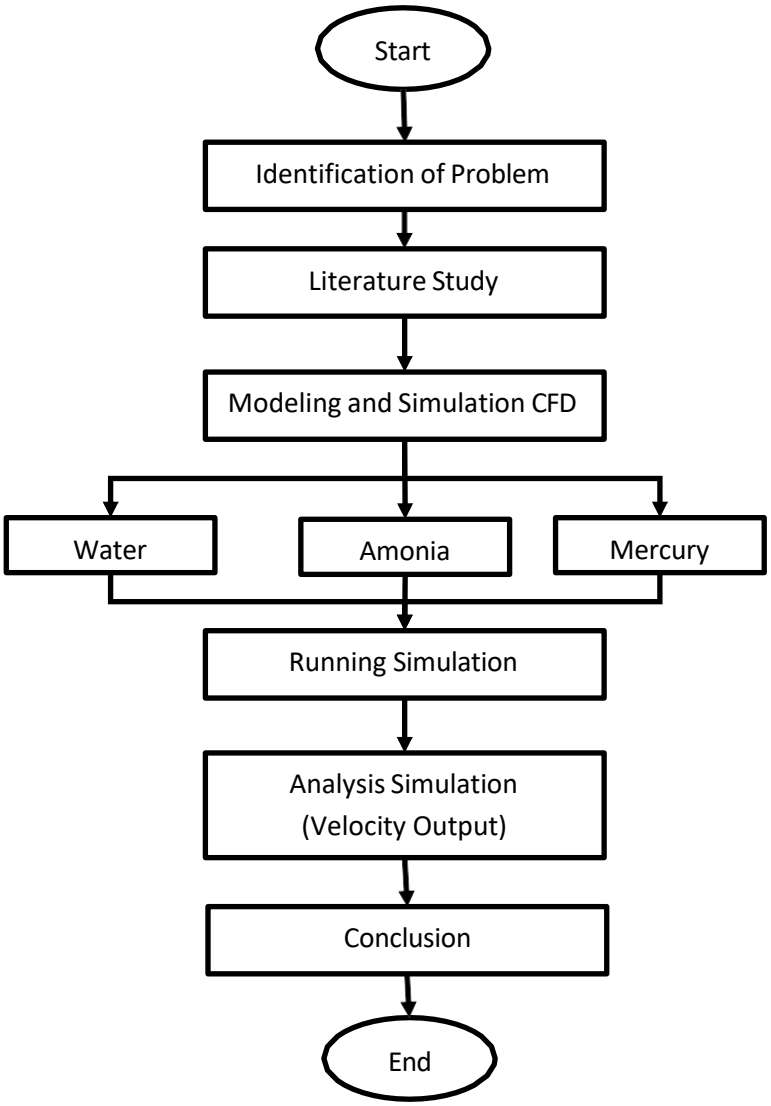


Figure 1. Flowchart the reserach

2.2 Desain Pipe

The pipe design in this CFD simulation is made in the form of a straight pipe with an elbow to analyze changes in flow characteristics when the fluid changes direction, as illustrated in Figure 2. The model has one inlet (marked in blue) as the fluid entry point and one outlet (marked in red) as the fluid exit point. The pipe geometry was created using CAD software, then imported into ANSYS Fluent for the simulation stage [21,22]. The inner surface of the pipe is assumed to be smooth so that the analysis focuses on the influence of the physical properties of the fluid, rather than the effects of surface roughness [23]. With this design, the distribution pattern of velocity and flow direction can be observed more realistically, resembling the conditions of piping in the industrial world.

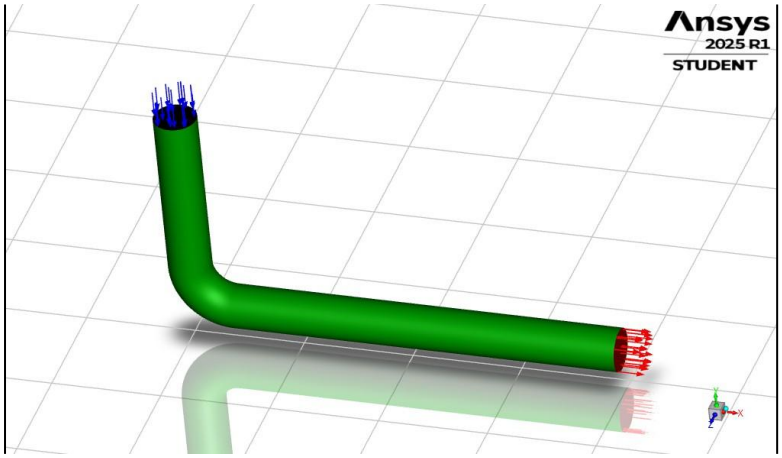


Fig. 2. Desain & boundary condition of the pipe

The boundary conditions applied include an inlet velocity of 0.52 m/s with a uniform flow profile, an outlet pressure of 0 Pa (gauge pressure), and a pipe wall with no-slip conditions and a smooth surface. The iteration process uses the SIMPLE algorithm for pressure-velocity coupling with double precision. The convergence criterion is set at a maximum residual value of 10^{-5} for the continuity and momentum equations. These settings are used consistently for all three types of fluids (water, ammonia, and mercury) to ensure that the simulation results can be fairly compared and reproduced by other researchers.

2.3 Equation

Simulations using ANSYS Fluent are based on the application of basic fluid conservation equations, which include the laws of mass, momentum, and energy conservation [24,25]. These equations explain the interaction between mass and forces that affect fluid flow behavior in pipes. In practice, ANSYS Fluent solves these equations numerically to determine the distribution of velocity, pressure, and overall flow characteristics [26]. Through this approach, a more detailed analysis can be performed on the influence of fluid physical properties such as density and viscosity on the shape and pattern of the flow [27,28]. Therefore, the simulation results provide a clear representation of the differences in the flow characteristics of water, ammonia, and mercury under the same conditions [29,30].

a. Continuity Equation (Mass Conservation)

$$\nabla \cdot (\rho \vec{v}) = 0 \quad (1)$$

Ensures that mass is conserved throughout the flow field.
Where:

ρ = fluid density (kg/m³)

$\vec{v}$ = velocity vector (m/s)

b. Momentum Equation (Navier–Stokes Equation)

$$\rho(\vec{v} \cdot \nabla \vec{v}) = -\nabla p + \mu \nabla^2 \vec{v} \quad (2)$$

Describes the balance of forces acting on the fluid, including pressure and viscous effects.
Where:

p = static pressure (Pa)

μ = dynamic viscosity (Pa·s)

These equations are automatically solved numerically by ANSYS Fluent to obtain the velocity distribution of each fluid

c. Reynolds Number (Flow Regime Indicator)

$$Re = \frac{\rho v D}{\mu} \quad (3)$$

Used to identify the type of flow (laminar or turbulent).
Where:

Re = Reynolds number (dimensionless)

v = average velocity (m/s)

D = pipe diameter (m)

Flow classification:

$Re < 2300$: Laminar

$2300 < Re < 4000$: Transitional

$Re > 4000$: Turbulent

d. Velocity Distribution in a Pipe (Laminar Flow)

For laminar flow in a circular pipe, the velocity profile follows the Hagen–Poiseuille equation:

$$v(r) = v_{max}\ (1 - \frac{r^2}{R^2}) \quad (4)$$

Where:

$v(r)$ = velocity at radial position r (m/s)

v_{max} = maximum velocity at the centerline (m/s)

R = radius of the pipe (m)
This equation shows that velocity decreases from the pipe center to zero at the wall due to viscous friction.

e. Relation Between Maximum and Average Velocity

$$v_{max} = 2v_{avg} \quad (5)$$

This relation is valid for laminar, fully developed flow in a circular pipe.
ANSYS Fluent can compute both v_{max} and v_{avg} values directly from simulation results.

f. Comparative Analysis

The velocity data obtained for each fluid were compared using:

$$Velocity\ Ratio = \frac{v_{avg,fluid}}{v_{avg,water}} \quad (6)$$

Where:

$v_{avg,fluid}$ = average velocity of the selected fluid (m/s)

$v_{avg,water}$ = average velocity of water (as reference)

This ratio helps visualize how the viscosity and density of each fluid influence its flow velocity in identical conditions.

3. Results and Discussion

3.1 Contour of the Pipe Result

Figure 3 presents the simulation results of fluid flow at a velocity of 0.05 m/s using ANSYS 2025 R1 Student, involving three types of fluids: water, ammonia, and mercury. Each fluid exhibits a velocity distribution represented by a color gradient from blue to red, where the red area indicates the highest flow velocity. Noticeable differences are observed in the flow patterns: water (a) demonstrates a more uniform flow due to its moderate viscosity, ammonia (b) shows a wider velocity spread because of its lower viscosity, while mercury (c) displays a narrower high-velocity region as a result of its higher density and viscosity. Overall, the simulation results indicate that variations in physical properties, particularly density and viscosity, significantly influence the flow distribution and behavior within the pipe.

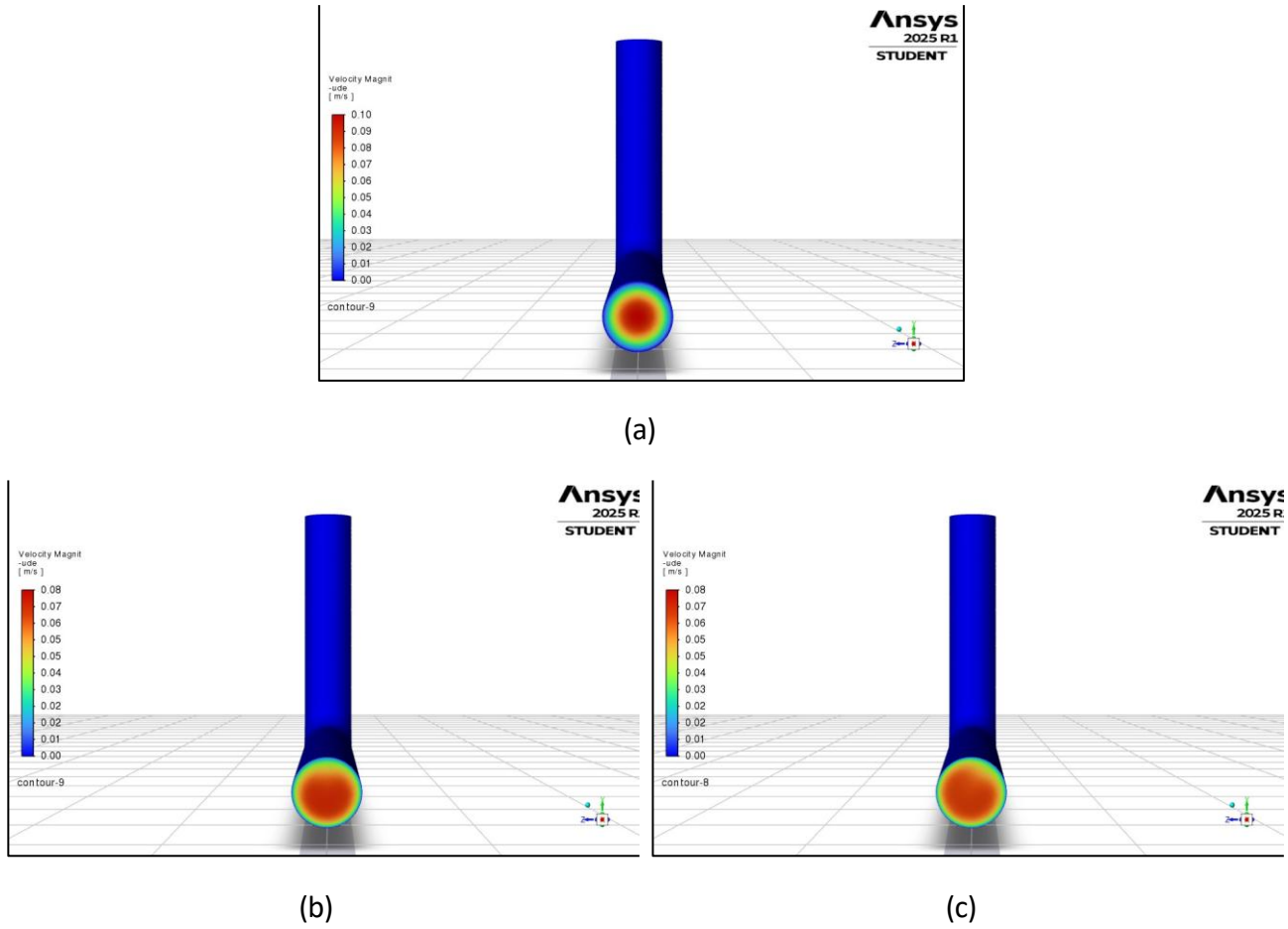
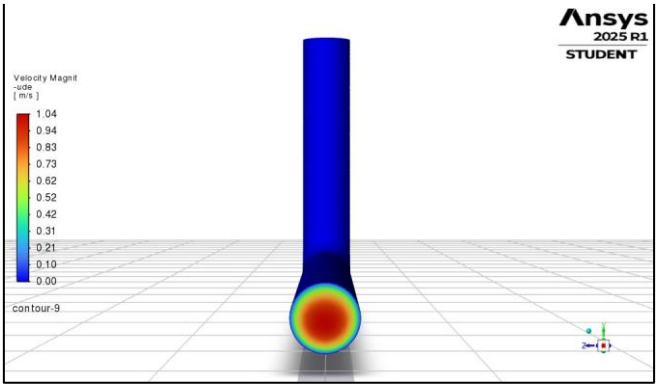
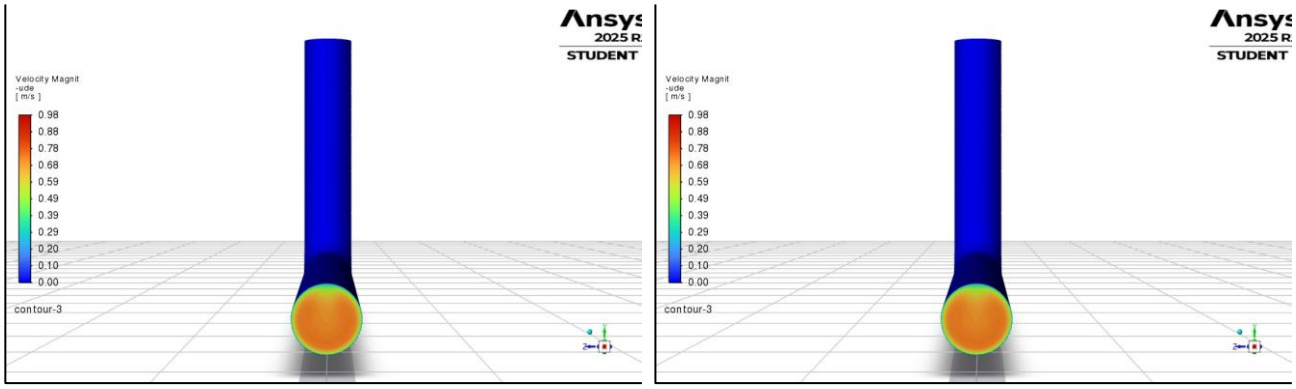


Fig. 3. Velocity 0.05 simulation in ANSYS: (a) Water 0.05 (b) Ammonia 0.05 (c) Mercury 0.05

Figure 4 presents the simulation results of fluid flow at a velocity of 0.64 m/s using ANSYS 2025 R1 Student, involving three types of fluids: water, ammonia, and mercury. The velocity distribution in each simulation is visualized through a colour gradient ranging from blue to red, with red indicating the highest flow velocity regions. Water (a) shows a relatively uniform and stable velocity pattern due to its moderate viscosity, while ammonia (b) reveals a broader and faster velocity distribution because of its lower viscosity and greater flow mobility. Conversely, mercury (c) displays a narrower high-velocity area caused by its high density and viscosity, suggesting stronger resistance to flow when compared to water and ammonia.



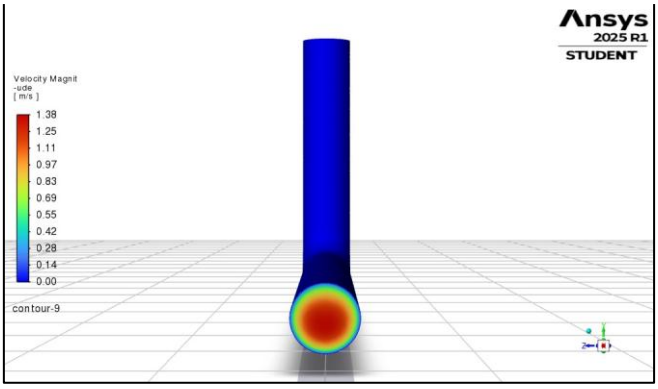
(a)



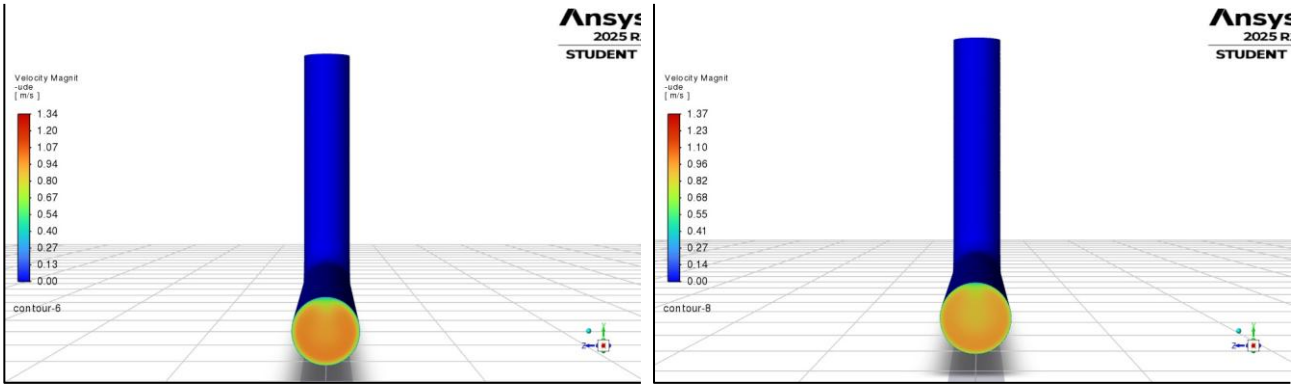
(b) (c)

Fig. 4. Velocity 0.64 simulation in ANSYS: (a) Water 0.64 (b) Ammonia 0.64 (c) Mercury 0.64

Figure 5 presents the simulation results of fluid flow at a velocity of 0.87 m/s using ANSYS 2025 R1 Student for three types of fluids: water, ammonia, and mercury. Each simulation illustrates the fluid velocity distribution using a color gradient from blue to red, where red indicates regions with the highest flow velocity. Water (a) shows a stable and uniform flow pattern, while ammonia (b) exhibits a greater increase in velocity due to its lower viscosity and higher flow mobility. In contrast, mercury (c) displays a narrower high-velocity region caused by its higher density and viscosity, resulting in greater flow resistance compared to water and ammonia.



(a)



(b) (c)

Fig. 5. Velocity 0.87 simulation in ANSYS: (a) Water 0.87 (b) Ammonia 0.87 (c) Mercury 0.87

3.2 Anova Statistical Results

The results summarized in Table 1 present the statistical data for the three tested fluids—water, ammonia, and mercury—along with the inlet velocity condition. Each fluid was measured three times, yielding nearly identical average velocity values around 0.52 m/s. The variance values, which are also very close for all samples, indicate that the simulation data are consistent and stable under identical boundary conditions. This similarity in the averages and variances suggests that the type of fluid has only a minor influence on the overall velocity magnitude when inlet velocity is maintained constant.

The statistical comparison using ANOVA, as shown in Table 2, further confirms that there is no significant difference in the outlet velocity among the three fluids. The calculated F-value of 1.33×10^{-7} is far below the critical F-value (4.07), and the P-value of 1 indicates that the variations in fluid types are statistically insignificant. This means that despite differences in physical properties such as density and viscosity, the average velocity at the outlet remains nearly the same for water, ammonia, and mercury. These findings demonstrate that, under identical simulation parameters, the influence of fluid type on average outlet velocity is minimal and can be considered negligible for engineering applications with uniform inlet conditions.

Table 1
Summary of fluid velocity data

Groups	*Count*	*Sum*	*Average*	*Variance*
inlet Velocity	3	1,56	0,52	0,1789
water	3	1,56028918	0,520096394	0,178958846
amonia	3	1,56065183	0,520217276	0,179049953
mercury	3	1,56026505	0,520088349	0,178933171

Table 2
ANOVA results for fluid velocity comparison

Source of Variation	*SS*	*df*	*MS*	*F*	*P-value*	*F crit*
Between Groups	7,1704E-08	3	2,39013E-08	1,33556E-07	1	4,066180551
Within Groups	1,431683942	8	0,178960493			
Total	1,431684014	11				

Based on these findings, an F value of 1.33×10^{-7} was obtained, while the critical F value ($F_{(}crit_{)}$) was 4.07. Since F is less than 0.05, it can be concluded that there is no statistically significant difference between the three types of fluids in terms of their outlet velocity. This means that variations in fluids (such as water, ammonia, and mercury) do not have a significant impact on the average outlet velocity according to the data from this simulation. However, even though the results are not statistically significant, the visualization and comparison of speed profiles still show patterns that can be understood physically.

3.2 Outlet Velocity Graph Analysis

The "Velocity Outlet" graph in Figure 6 presents the numerical comparison of outlet velocities for three different fluids—water, ammonia, and mercury—at three observation points along the pipe. The velocity values recorded for mercury were 0.0500 m/s, 0.8700 m/s, and 0.6401 m/s, showing that it consistently produced the highest flow speed, especially at the second point where the peak velocity occurred. This trend demonstrates that mercury's high density and momentum contribute to its ability to accelerate rapidly in the middle section before slowing slightly near the outlet due to viscous resistance. Overall, these results indicate that mercury experiences the most significant variation in flow velocity, reflecting the impact of its large mass and kinetic energy on the overall flow dynamics.

In comparison, ammonia and water display lower but relatively consistent velocity patterns across the same observation points. Ammonia recorded velocities of 0.0500 m/s, 0.8703 m/s, and 0.6403 m/s, while water exhibited 0.0500 m/s, 0.8702 m/s, and 0.6401 m/s, respectively. The small difference between ammonia and water (approximately 0.0002 m/s) indicates that both fluids have nearly similar flow characteristics when subjected to identical boundary conditions. However, ammonia's lower viscosity allows for slightly higher flow acceleration compared to water, which maintains a smoother and more stable velocity profile along the pipe length. These results collectively confirm that, under constant inlet velocity, variations in density and viscosity only cause minor differences in outlet flow behavior among the tested fluids.

Overall, the order of average flow velocity from highest to lowest is ammonia > water > mercury. This trend reinforces the physical interpretation that viscosity and density play a limited but predictable role in determining fluid velocity under equal inlet conditions. Fluids with lower viscosity, such as ammonia, tend to experience less wall friction and thus achieve slightly higher speeds, while denser fluids like mercury flow more slowly due to greater inertial resistance. In general, these findings emphasize that, within the same simulation setup, the influence of fluid type on the average flow velocity in the pipe is minimal, and the small observed variations remain consistent with theoretical expectations of each fluid's physical properties.

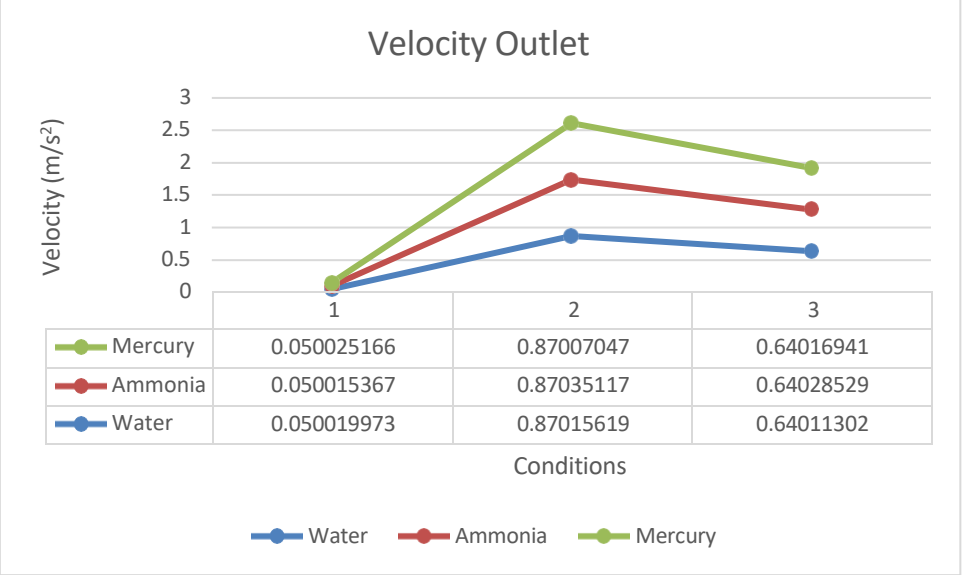


Fig. 6. Comparation of the output velocity

3.4 Analysis of Reynolds Number (Re) and Flow Regime

To quantitatively characterize the flow regime, the Reynolds Number (*Re*) was calculated using Equation (3), $Re = \frac{\rho v D}{?}$. The hydraulic diameter (*D*) of the pipe was specified as 0.0127 meters. The fluid properties and the simulated average velocity (*v*) were used for the calculation, as summarized in Table 3.

Table 3
Fluid physical properties used in the simulation (assumed at room temperature)

Fluid	Density (ρ)(kg/m³)	Dynamic Viscosity (μ)(Pa·s)
Water (H_2O)	997	8.9×10^{-4}
Ammonia (NH_3)	600	1.5×10^{-4}
Mercury (Hg)	13,534	1.52×10^{-3}

The results of the Reynolds Number calculation, based on the defined hydraulic diameter, are presented in Table 4.

Table 4
Results of Reynolds Number calculation and flow regime determination (D=0.0127 m)

Fluid	Average Velocity (*v*) (m/s)	Reynolds Number (*Re*)	Flow Regime
Water (H_2O)	0.520096	7,595	Turbulent (*Re* > 4000)
Ammonia (NH_3)	0.520217	26,423	Turbulent (Re > 4000)
Mercury (Hg)	0.520088	56,922	Highly Turbulent (Re > 4000)

The results in Table 4 conclusively show that due to the relatively large hydraulic diameter (0.0127 m), the flow for all three fluids is firmly established in the Turbulent regime (*Re* > 4000).

1. Water (*Re*≈ 7,595): The Reynolds number is significantly above the transition boundary, indicating a fully turbulent flow, characterized by intense mixing and a flatter velocity profile near the pipe centre compared to laminar flow.

2. Ammonia (Re ≈ 26,423): Ammonia exhibits the highest Reynolds number among the three, primarily due to its combination of high velocity and very low viscosity. This represents highly chaotic and high-inertia flow, resulting in the most significant wall shear stress.
3. Mercury (Re ≈ 56,922): Despite its relatively high viscosity, Mercury's extremely high density drives its Reynolds number to the highest value, indicating the most vigorous turbulent mixing.

This finding suggests that the slight variations in velocity observed among the fluids (as discussed in Section 3.2) are not related to a change in the flow regime (e.g., from laminar to turbulent) but rather to the different degrees of turbulence intensity, which are governed by the inherent physical properties ($\rho \ and \ \mu$ of each fluid. The highly turbulent nature of all flows implies that momentum transfer is dominated by inertial forces rather than viscous ones.

4. Conclusion

Based on the findings from numerical simulations conducted using ANSYS Fluent, the three types of fluids, namely water, ammonia, and mercury, showed almost the same average velocity in the outlet pipe. The average values of the velocities of the various fluids were 0.52009639 m/s for water, 0.52021728 m/s for ammonia, and 0.52008835 m/s for mercury. The difference in these velocity values is very minimal, with the highest difference being around 0.00012893 m/s or 0.0248% between the various types of fluids. Therefore, it can be quantitatively concluded that changes in fluid type do not have a significant effect on the average flow velocity. This condition illustrates that in a simulation setting with equal inlet velocity, the density and viscosity properties of the fluid only have a minor effect on the average velocity at the pipe outlet.

Physically, this phenomenon can be understood through the basic characteristics of fluid flow in pipes. In internal flow systems, the average velocity of the fluid is influenced by the inlet pressure that drives it and the frictional forces caused by viscosity on the pipe surface. Ammonia, which has the lowest viscosity compared to the other two fluids, produces less friction, so its flow is slightly faster than water and mercury. On the other hand, mercury has a much higher density, but because the inlet pressure remains stable, the kinetic energy per unit mass is quite low, so its average velocity is slightly lower. However, the velocity distribution within the cross-section may still vary between different fluids due to differences in their viscosity and Reynolds numbers.

Based on the velocity output graph, it can be seen that the velocity distribution pattern among fluids shows the same trend, where the highest velocity is usually located in the centre of the pipe and decreases towards the wall side due to the influence of the boundary layer. This is in line with the idea of a velocity pattern for laminar flow expressed as $v(r) = v_{max} \ (1 - \frac{r^2}{R^2})$, where (v_{max} is the highest velocity occurring in the center of the pipe and (R) is the pipe radius. is the maximum velocity at the center of the pipe and (R) is the pipe radius. Although simulations show small variations in peak velocity numbers, the overall average values are still nearly similar due to the mutually neutralizing effects of viscosity across the cross-sectional area. Therefore, the existing flow will be distributed evenly and stably among various types of fluids.

In general, the results of this simulation show that the impact of fluid variations on the average velocity in a pipe is very small, especially when boundary conditions such as inlet pressure and initial velocity are set to be the same. The main factors that can cause greater velocity differences are not only due to the type of fluid, but also to a combination of viscosity, density, and flow conditions (whether laminar or turbulent). Therefore, to create a more pronounced difference in velocity between fluids, it is important to adjust other factors such as pressure difference, temperature, or

pipe size. This conclusion emphasizes that considering the physical characteristics of fluids in flow system studies is important, but also shows that under certain circumstances, these variations can be ignored without significantly affecting the average velocity calculation results.

Future research should focus on expanding the current study by examining how variations in pipe geometry, inlet velocity, and surface roughness influence the flow characteristics of fluids with different densities and viscosities. Further investigation into temperature-dependent viscosity effects could reveal how thermal gradients alter velocity distribution and pressure drop in practical systems. Additionally, incorporating turbulent flow modelling and experimental validation, such as pressure-drop measurements or flow visualization—would strengthen the reliability of the CFD results. Such improvements will not only address the current study's limitations but also provide a more comprehensive understanding of fluid flow behaviour in industrial piping systems, enabling more accurate design and energy-efficient operation.

References

[1] Patel, Manvendra, Rahul Kumar, Kamal Kishor, Todd Mlsna, Charles U. Pittman Jr, and Dinesh Mohan. "Pharmaceuticals of emerging concern in aquatic systems: chemistry, occurrence, effects, and removal methods." *Chemical reviews* 119, no. 6 (2019): 3510-3673. https://doi.org/10.1021/acs.chemrev.8b00299

[2] Ahmad, Fiaz, Daochen Zhu, and Jianzhong Sun. "Environmental fate of tetracycline antibiotics: degradation pathway mechanisms, challenges, and perspectives." *Environmental Sciences Europe* 33, no. 1 (2021): 64. https://doi.org/10.1186/s12302-021-00505-y

[3] Belete, Biniam, Belay Desye, Argaw Ambelu, and Chalachew Yenew. "Micropollutant removal efficiency of advanced wastewater treatment plants: a systematic review." *Environmental Health Insights* 17 (2023): 11786302231195158. https://doi.org/10.1177/11786302231195

[4] Hunge, Yuvaraj M., A. Yadav, and B. Mohite. "Basics of photocatalysis and different strategy for enhancing the photocatalytic efficiency." *American Journal of Engineering and Applied Sciences* 13, no. 2 (2020): 265-268. https://doi.org/10.3844/ajeassp.2020.265.268

[5] Liu, Hang, Chengyin Wang, and Guoxiu Wang. "Photocatalytic advanced oxidation processes for water treatment: recent advances and perspective." *Chemistry–An Asian Journal* 15, no. 20 (2020): 3239-3253. https://doi.org/10.1002/asia.202000895

[6] Mahmud, Md, and Md Sohanur Rahman. "A Concise Review on Applications of Nickel Oxide Nanoparticles and Their Extraction Parts." *International Journal of Advanced Biological and Biomedical Research* 13, no. 3 (2025): 317-340. https://doi.org/10.48309/IJABBR.2025.2042688.1546[7] Raju, Kumar, Saravanan Rajendran, Tuan KA Hoang, D. Durgalakshmi, Jiaqian Qin, D. E. Diaz-Droguett, F. Gracia, and M. A. Gracia-Pinilla. "Photosynthesis of H2 and its storage on the bandgap engineered mesoporous (Ni2+/Ni3+) O@ TiO2 heterostructure." *Journal of Power Sources* 466 (2020): 228305. https://doi.org/10.1016/j.jpowsour.2020.228305

[8] Wang, Yaquan, and Yao Lu. "Sodium alginate-based functional materials toward sustainable applications: water treatment and energy storage." *Industrial & Engineering Chemistry Research* 62, no. 29 (2023): 11279-11304. https://doi.org/10.1021/acs.iecr.3c01082

[9] Albarelli, Juliana Q., Diego T. Santos, Sharon Murphy, and Michael Oelgemöller. "Use of Ca–alginate as a novel support for TiO2 immobilization in methylene blue decolorisation." *Water Science and Technology* 60, no. 4 (2009): 1081-1087. https://doi.org/10.2166/wst.2009.459

[10] Rocher, Vincent, Agnès Bee, Jean-Michel Siaugue, and Valérie Cabuil. "Dye removal from aqueous solution by magnetic alginate beads crosslinked with epichlorohydrin." *Journal of hazardous materials* 178, no. 1-3 (2010): 434-439. https://doi.org/10.1016/j.jhazmat.2010.01.100

[11] Monroy, Luis Hernandez, Jason Robert Tavares, and Marie-Josee Dumont. "Photodegradation of ciprofloxacin using an alginate/TiO2 hydrogel for water remediation." *Journal of Environmental Chemical Engineering* 13, no. 2 (2025): 115868. https://doi.org/10.1016/j.jece.2025.115868

[12] Manohara, Halanur M., Sooraj S. Nayak, Gregory Franklin, Sanna Kotrappanavar Nataraj, and Dibyendu Mondal. "Progress in marine derived renewable functional materials and biochar for sustainable water purification." *Green Chemistry* 23, no. 21 (2021): 8305-8331. https://doi.org/10.1039/D1GC03054J

[13] Sohrabi, Somayeh, Mostafa Keshavarz Moraveji, and Davood Iranshahi. "A review on the design and development of photocatalyst synthesis and application in microfluidic reactors: Challenges and opportunities." *Reviews in Chemical Engineering* 36, no. 6 (2020): 687-722. https://doi.org/10.1515/revce-2018-0013

[14] Zhu, Shasha, and Dunwei Wang. "Photocatalysis: basic principles, diverse forms of implementations and emerging scientific opportunities." *Advanced Energy Materials* 7, no. 23 (2017): 1700841. https://doi.org/10.1002/aenm.201700841
[15] Nezamzadeh-Ejhieh, Alireza, and Arezoo Shirzadi. "Enhancement of the photocatalytic activity of ferrous oxide by doping onto the nano-clinoptilolite particles towards photodegradation of tetracycline." *Chemosphere* 107 (2014): 136-144. https://doi.org/10.1016/j.chemosphere.2014.02.015
[16] Galedari, Mona, Mohsen Mehdipour Ghazi, and Seyed Rashid Mirmasoomi. "Photocatalytic process for the tetracycline removal under visible light: presenting a degradation model and optimization using response surface methodology (RSM)." *Chemical Engineering Research and Design* 145 (2019): 323-333. https://doi.org/10.1016/j.cherd.2019.03.031
[17] Mamaghani, Alireza Haghighat, Fariborz Haghighat, and Chang-Seo Lee. "Photocatalytic oxidation of MEK over hierarchical TiO2 catalysts: Effect of photocatalyst features and operating conditions." *Applied Catalysis B: Environmental* 251 (2019): 1-16. https://doi.org/10.1016/j.apcatb.2019.03.057
[18] Fosso-Kankeu, Elvis, Sadanand Pandey, and Suprakas Sinha Ray, eds. Photocatalysts in advanced oxidation processes for wastewater treatment. John Wiley & Sons, 2020. https://doi.org/10.1002/9781119631422
[19] Sapawe, Norzahir. "Hybridization of zirconia, zinc and iron supported on HY zeolite as a solar-based catalyst for the rapid decolorization of various dyes." *New Journal of Chemistry* 39, no. 6 (2015): 4526-4533. https://doi.org/10.1039/C4NJ02424A
[20] Cheah, Kingsly Tian Chee, and Jing Yao Sum. "Synthesis and evaluation of Fe-doped zinc oxide photocatalyst for methylene blue and congo red removal." *Progress in Energy and Environment* (2022): 13-28. https://doi.org/10.37934/progee.22.1.1328
[21] Saadati, Farzaneh, Narjes Keramati, and Mohsen Mehdipour Ghazi. "Influence of parameters on the photocatalytic degradation of tetracycline in wastewater: a review." *Critical reviews in environmental science and technology* 46, no. 8 (2016): 757-782. https://doi.org/10.1080/10643389.2016.1159093
[22] Khairol, Nurul Fahmi, Norzahir Sapawe, and Mohamed Danish. "Effective photocatalytic removal of different dye stuffs using ZnO/CuO-incorporated onto eggshell templating." *Materials Today: Proceedings* 19 (2019): 1255-1260. https://doi.org/10.1016/j.matpr.2019.11.130
[23] Gopal, Geetha, Namrata Roy, Natarajan Chandrasekaran, and Amitava Mukherjee. "Photo-assisted removal of tetracycline using bio-nanocomposite-immobilized alginate beads." *ACS omega* 4, no. 17 (2019): 17504-17510. https://doi.org/10.1021/acsomega.9b02339
[24] Mokif, Layla Abdulkareem, and Ayad AH Faisal. "Laboratory studies into Tetracycline removal from aqueous solutions by beads of calcium-Iron oxide nanoparticles." *Water, Air, & Soil Pollution* 234, no. 8 (2023): 556. https://doi.org/10.1007/s11270-023-06585-1
[25] Fatimah, Is, Rico Nurillahi, and Fitriana Harjanti. "Hydrothermal synthesized zinc oxide/kaolinite for photo-decolorization of methyl violet." *Desalination and Water Treatment* 185 (2020): 286-295. https://doi.org/10.5004/dwt.2020.25343
[26] Fauzi, A. A., A. A. Jalil, M. Mohamed, N. A. Naseri, C. N. C. Hitam, N. F. Khusnun, N. S. Hassan, A. F. A. Rahman, F. F. A. Aziz, and M. S. M. Azmi. "Fibrous silica induced narrow band gap TiO2 catalyst for enhanced visible light-driven photodegradation of methylene blue." In *IOP Conference Series: Materials Science and Engineering*, vol. 808, no. 1, p. 012016. IOP Publishing, 2020. https://doi.org/10.1088/1757-899X/808/1/012016